

UNCLASSIFIED



Australian Government
Department of Defence
Defence Science and
Technology Organisation

Strong Magnetic Field Characterisation

John Waschl and Jonathan Schubert¹

Weapons Systems Division
Defence Science and Technology Organisation

¹**Adelaide University**

DSTO-TR-2699

ABSTRACT

Three magnetic field sources were characterised through a combination of selected measurement and subsequent modelling. Detailed spatial and temporal field distributions were developed as a consequence. The results provided a basis from which to develop hardware for use in pulsed-power experiments.

RELEASE LIMITATION

Approved for public release

UNCLASSIFIED

UNCLASSIFIED

Published by

*Weapons Systems Division
DSTO Defence Science and Technology Organisation
PO Box 1500
Edinburgh South Australia 5111 Australia*

*Telephone: (08) 7389 5555
Fax: (08) 7389 6567*

*© Commonwealth of Australia 2012
AR-015-291
April 2012*

APPROVED FOR PUBLIC RELEASE

UNCLASSIFIED

UNCLASSIFIED

Strong Magnetic Field Characterisation

Executive Summary

There was a requirement to develop reasonably strong (~ 1 T), sufficiently long lived (~ 100 μ s) magnetic fields for experiments investigating interactions between hot gases from a detonation and the magnetic field.

The present investigation explored the utility of a rare earth permanent magnet and electromagnets as sources. Two electromagnet sources were constructed (a single coil and a Helmholtz like pair of coils). These coils were driven by a pulsed-power system to generate the fields. All the sources were characterised through a series of measurements and modelling. The goal was to develop a sufficiently representative spatial and temporal model that could be used as input to magnetohydrodynamic modelling.

A model of the magnet was developed and this compared well with data within a small measurement region. The coil models also proved reasonable representations. It was determined that a ~ 1 T field could be constructed near the single coil electromagnet for approximately 78 μ s. A smaller field of ~ 0.4 T was achieved with the Helmholtz like pair. The model also showed that our system was probably at the limit of our capability for producing intense fields, particularly for the Helmholtz like pair. The spatial distribution of the fields was predicted. Temporal distributions were also generated for the coils. Options for further investigation were provided.

UNCLASSIFIED

UNCLASSIFIED

This page is intentionally blank

UNCLASSIFIED

Authors

John Waschl

Weapons Systems Division

John Waschl is a physics graduate from Melbourne University. He also has post graduate qualifications in Audiology and Computer Simulation. After a brief period in private industry he joined DSTO in 1982. Since then he has worked mostly in the field of warheads and warhead effects. During his career he has been posted to Harry Diamond Laboratories (USA), British Aerospace Australia, and Office of Naval Research (USA). He currently leads the Weapons Effects Group at DSTO.

Jonathan Schubert

Contractor

Jonathon Schubert completed a B.Eng(Mechanical & Aerospace) (Honours) and B.Sc(Physics & Maths) from Adelaide University in 2011. During the summer of 2009 and then on a part-time basis thereafter, he worked in the Weapons Effects Group on modelling magnetic field distributions and assisted in associated experiments. His research interests have included using finite element analysis software to model electromagnetic field distributions in 3D.

UNCLASSIFIED

This page is intentionally blank

UNCLASSIFIED

Contents

1. INTRODUCTION.....	1
2. EXPERIMENT	2
3. RESULTS	4
3.1 Coordinate system	4
3.2 Permanent magnet field measurements	5
3.3 Electromagnet field measurements	6
3.4 Modelling	8
4. DISCUSSION	15
5. CONCLUSION	16
6. ACKNOWLEDGEMENTS	16
7. REFERENCES	17
APPENDIX A: COMSOL INPUT FILE FOR ALL MODELS.....	18

This page is intentionally blank

1. Introduction

Experiments where a magnetic field has been used to interact with the rapidly expanding hot gases from a detonation have been conducted. These gases are ionised and should therefore respond to the presence of the magnetic field. To explore this phenomenon knowledge of both the spatial and temporal distribution of the magnetic field are important and there is potential to adjust this distribution depending on available field sources. Two separate sources were available: static permanent magnetic fields and dynamic electromagnetic fields.

Other constraints implicit in the experiments were that the sources should be reasonably strong (~ 1 T), sufficiently long lived (~ 100 μ s), and not interfere with the normal flow of the gases. These restrictions meant that the design of the sources required some investigation.

The desired field strength was based on assessments [1] from preliminary magnetohydrodynamic (MHD) modelling and while not achievable by strong rare earth permanent magnets, the fields available from these magnets are reasonable over small regions and have the added advantage of simplifying the experimental setup as the field is always on. Electromagnets can be used to create larger and stronger fields of either short or long duration. Strong, long duration electromagnetic fields require sustained high currents and specialised cooling systems. Such systems were considered unnecessarily complicated for our purposes. The alternative of short duration electromagnetic fields means that precision timing is required to coordinate the arrival of the hot gases with the maximal field. The process of creating such a magnetic field is also complicated, requiring the use of a pulsed-power system (PPS) or even flux compression. A PPS was chosen for convenience.

Limiting the physical interference between the normal gas flow and any field generator is another issue to be addressed. Two approaches were selected based on the field generators available. One approach employs a magnet or electromagnet with the dipole moment arranged parallel to the flow. In this case the flow freely interacts with the field until it is impeded when making physical contact with the magnet or coil. The downside of this arrangement is that the strongest field parallel to the flow only occurs at the moment of physical contact. An alternative is to use two coils in a Helmholtz-like arrangement where the dipole is perpendicular to the flow and is present in the gap between the coils. Provided the gap is large enough, physical contact effects can be separated from the field effects.

Each of these sources required characterisation in order to compliment an interpretation of any observed interaction responses between the field and the detonation products and also to provide input to MHD modelling. A combination of measurement and subsequent modelling were used to achieve the characterisation. Measurement is relatively easy for the static field and therefore a reasonably dense matrix of measurement locations was used. For the dynamic field, a sparse number of measurements were taken. For both cases the measurements were used to verify the modelling in order to interpolate and extrapolate into the domain of interest. This paper describes the methodology and analysis used to characterise the magnetic fields.

The next section describes the experiments and the modelling approach. Section three provides results. Discussion of the results is presented in section four and conclusions in section five.

2. Experiment

Strong disc rare earth magnets [2] with an advertised surface field of approximately 0.5 T were used to supply the static magnetic field source. The disc magnet had a diameter of 50 mm and a thickness of 25 mm. The magnetic field surrounding this magnet was measured as shown in Figure 1. The field was measured using a longitudinal or axial (single axis) sensor probe attached to a Bell 5180 Telsameter [3] in a 3 dimensional 20 mm grid pattern from 0 to 100 mm standoff. The teslameter has a frequency response of DC- 30 kHz and can measure field strengths to ~3 T.

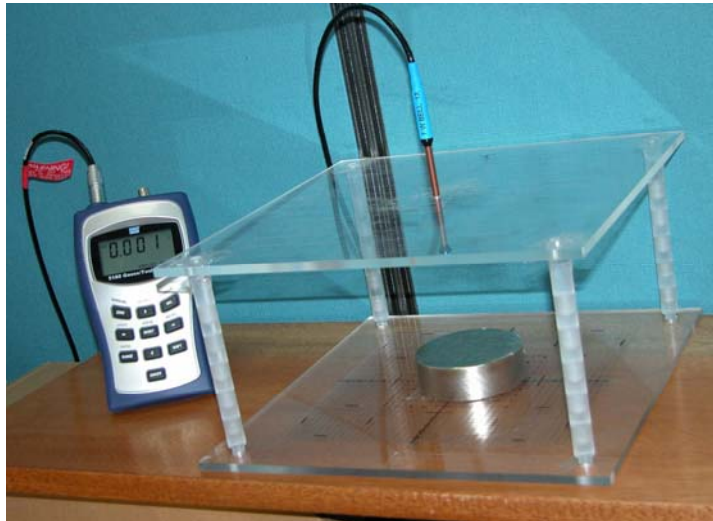


Figure 1. Rare earth disc magnet undergoing field measurement

A PPS [4] was used to generate the non stationary magnetic field. The PPS employed up to fifteen 200 μ F Maxwell model number 33778 10 kV capacitors connected in parallel. The energy stored on the capacitors was dumped through a spark gap switch into a range of coil windings. The PPS is capable of delivering >100 kA in less than 200 μ s depending on the voltage and total system capacitance, inductance, and resistance. The PPS also employs a clamping diode to prevent reverse current in the capacitors. A part of the system is shown in Figure 2. A Rogowski coil was used to measure the discharge current into the coil. Cigweld Transarc Super-flex cable was used for the coils. This cable can carry 790 A @ 30% duty cycle for a 60^o temperature rise. Two coil configurations were constructed for this study and these are listed in Table 1. While more precise solid coil configurations could have been constructed, it was decided that these flexible cables provided easier construction and were more suited to the destructive explosive environment for these initial investigations.



Figure 2. The picture shows some of the components of the PPS. In the foreground are 5 vertically stacked capacitors above which sits safety and control features. The left rear shows the diode clamp and the cylindrical spark gap switch.

Table 1. Coil descriptions

Coil type	Diameter (mm)	Turns	Number of coils	Separation of coils (mm)	Comment
A	265	2	1	-	Single vertical coil
B	265	3	2	310	Two horizontal coils

The field measurements for the electromagnet were made using two three axis Hall sensors [5] and the teslameter. The wide dynamic range of the teslameter probe allowed it to be placed close to the source. The available Hall sensors provide a dynamic measurement within approximately ± 7.3 mT and therefore required a standoff distance of about 500 mm to avoid saturation. All sensors were placed in a holder as shown in Figure 3. The teslameter probe was placed in the central location while the Hall sensors were either left and right or above and below that location. For these measurements the teslameter could only provide peak field values while the Hall sensors supplied continuous data with frequency content up to 100 kHz. Data was recorded on TEK TDS 784C and 684A.

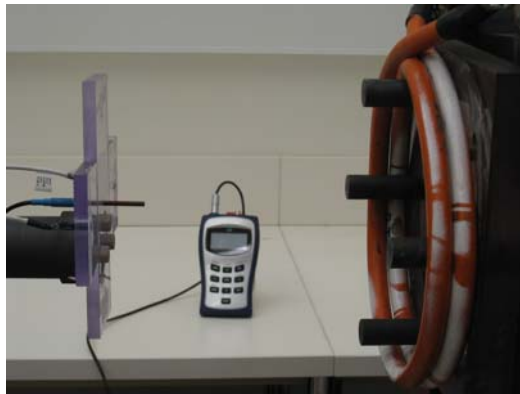


Figure 3. Type B coil and measurement fixture

The intention was to use all the measured data as a guide for the modelling. The output from the tuned model would then be used to determine the field at any point in the vicinity of the coils. COMSOL [6] was used as the modelling package to determine the spatial and temporal extent of the magnetic field. COMSOL is a modelling tool suitable for an electromagnetic problem and requires geometrical and current density input. For this investigation COMSOL Version 3.5a with AC/DC Module was implemented on a dual core Intel Xeon Processor (2.80 GHz) with 24 GB DDR3 RAM, and a Microsoft Windows XP, x64 Professional Edition OS.

3. Results

3.1 Coordinate system

For the permanent magnet the origin is the centre of the top face of the magnet as shown in Figure 4. XZ is in the page plane and the y axis is into the page.

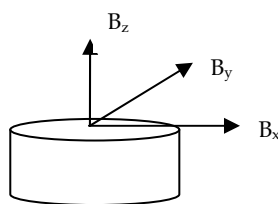


Figure 4. Magnetic field vector definition over a single permanent magnet

For the coils the origin was taken as the centre of the front face of the type A coil and the centre of the centreline between the two coils for the type B coil. Figure 5 is a schematic showing the XY plane where the z axis is into the page.

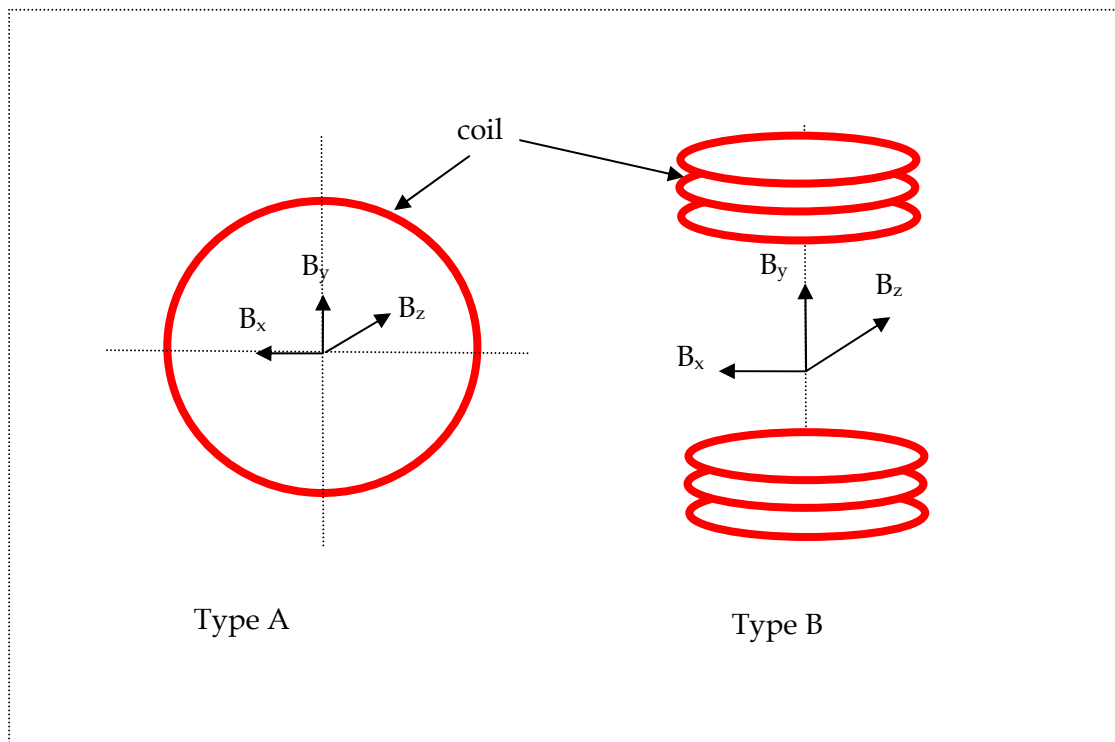


Figure 5. Axes for Type A and B coils. The view is as seen from the Hall sensor.

3.2 Permanent magnet field measurements

Table 2 shows the magnetic field components (B_x , B_y , and B_z) as a function of position at 20 mm intervals. Two planes are shown: XY plane at $z=0$ in Table 2a and XY plane at $z=20$ mm in Table 2b. The plane at $z=0$ refers to the plane parallel to and coincident with the surface of the magnet. For these measurements the probe tip sensor offset of 1.25 mm was ignored.

Table 2. Measured magnetic field as a function of position in XY plane at a) $z = 0$ and b) $z = 20$ for the disc magnet. Four measurement locations are shown for each z value.

a)

Magnetic field (mT)	Position (mm)			
	0,0,0	20,0,0	40,0,0	60,0,0
B_x	-36.7	-303	-90.1	-19.6
B_y	-23.5	-15.4	2.7	1.3
B_z	-449	-495	52	22
B_{total}	451.1	580.6	104.1	29.5

b)

Magnetic field (mT)	Position (mm)			
	0,0,20	20,0,20	40,0,20	60,0,20
B_x	-9.8	-68.5	-52.1	-22.5
B_y	-9.4	-5.4	-0.9	0.2
B_z	-165	-109.9	-19.9	2.9
B_{total}	165.6	129.6	55.8	22.7

3.3 Electromagnet field measurements

At discharge, the sudden rise and subsequent ringdown of the current through the coil is dependent on the circuit characteristics. Sample raw data for the current discharge trace (from the Rogowski coil) and the associated 3 axis Hall response is shown in Figure 6. The Hall sensors have a 2500 mV bias to allow for positive and negative field measurement.

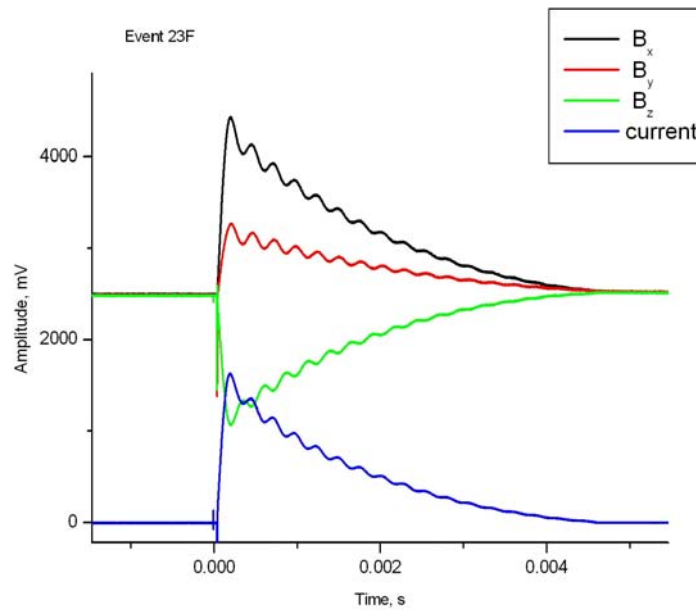


Figure 6. Example current ringdown ($100\ 0\mu\text{F}$ @ $9\ \text{kV}$) and Hall sensor response (B_x , B_y , B_z) following discharge from the pulsed-power system into type A coil.

Table 3 provides the magnetic field values (at designated locations) for the two coil types used together with the peak current measurements. A number of the measurements are not total field. The PPS consisted of $1000\ \mu\text{F}$ charged to a maximum of $10\ \text{kV}$.

Table 3. Measured current and magnetic field values at various locations for coil types A and B when connected to 1000 μ F and charged up to 10 kV.

Coil type	x (mm)	y (mm)	z (mm)	B _{total} at (x,y,z) (mT)	Current (kA)
A	100	0	-680	9.5	83
A	100	0	-680	9.3	79
A	0	100	-680	9.9	83
A	0	100	-680	10.2	90
A	-100	0	-680	11.2	83
A	-100	0	-680	11.2	79
A	0	-100	-680	10.8	83
A	0	0	0	1020 ¹	93
A	0	0	0	1020 ¹	93
A	0	0	-260	94 ¹	93
B	100	0	-510	8.6	99
B	100	0	-510	9.1	104
B	100	0	-510	8.8	95
B	0	100	-510	10.4	97
B	-100	0	-510	11.1	99
B	-100	0	-510	11.1	104
B	-100	0	-510	11.4	95
B	0	-100	-510	10.9	97
B	0	-100	-510	11.2	97
B	0	-100	-510	11.2	96
B	0	0	0	301 ²	95
B	0	0	0	295 ²	95
B	0	0	-75	307 ³	95
B	0	155	0	697 ²	95
B	0	-155	0	667 ²	95

3.4 Modelling

It was assumed that the disc magnet could be represented by a thick current carrying coil with a radius (r) less than the magnet radius. Initial current (i) and number of turns (N) were determined by analytic estimates of B_z where z is the distance along the centreline from the centre of the magnet and μ_0 is the permeability of free space:

$$B_z(0,0,z) = \frac{\mu_0 N i r^2}{2(r^2 + z^2)^{3/2}} \quad (1)$$

¹ B_z measured, but other components zero.

² B_y measured, but other components zero.

³ B_y measured, but other components expected to be small.

Good agreement with B_z along the z axis was found for $i=60$ kA and $r=20$ mm with a coil thickness of 10 mm. These values formed the starting point for the COMSOL modelling.

Having determined all initial conditions, a trial and error approach was used to achieve a match within the half space above the surface of the magnet. A strict minimum was not found, however, the trend indicated that $i=200$ kA, $r=25$ mm, and using a fine mesh provided a good match and a comparison between the calculated field and the measured field at a number of locations as shown in Figure 7. Details on the final COMSOL input files are provided in Appendix A.

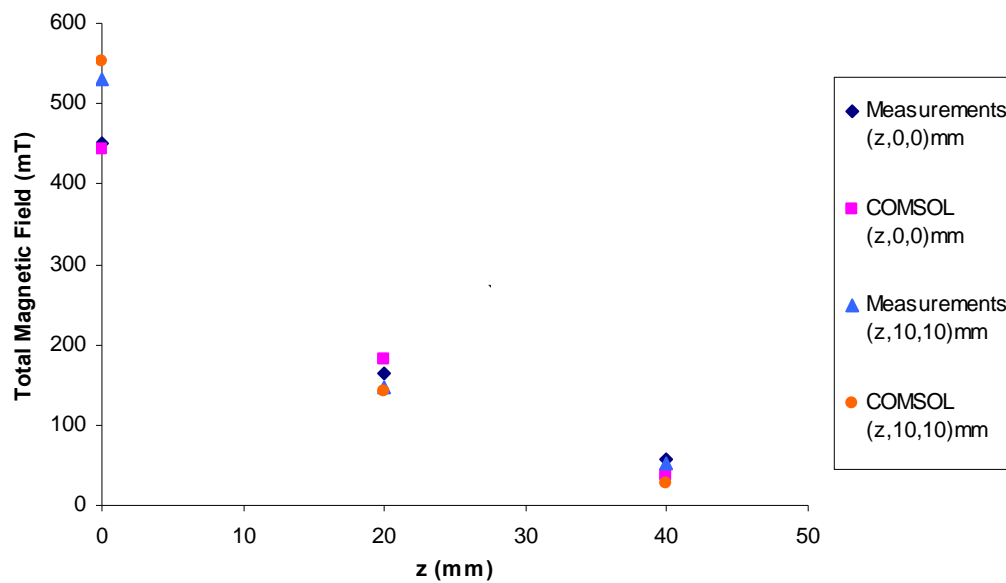


Figure 7. Comparison between COMSOL model and measured field data for the disc magnet. Data are shown for $(z,0,0)$ and $(z,10,10)$.

A typical output from the model of the magnet is shown in Figure 8 where the coil is shown in grey and the field vectors are shown as red arrows. The colour bar indicates the magnetic field strength set to an arbitrary 0.25 T. The white area has a field >0.25 T. The size of the arrow is proportional to the strength of the field.

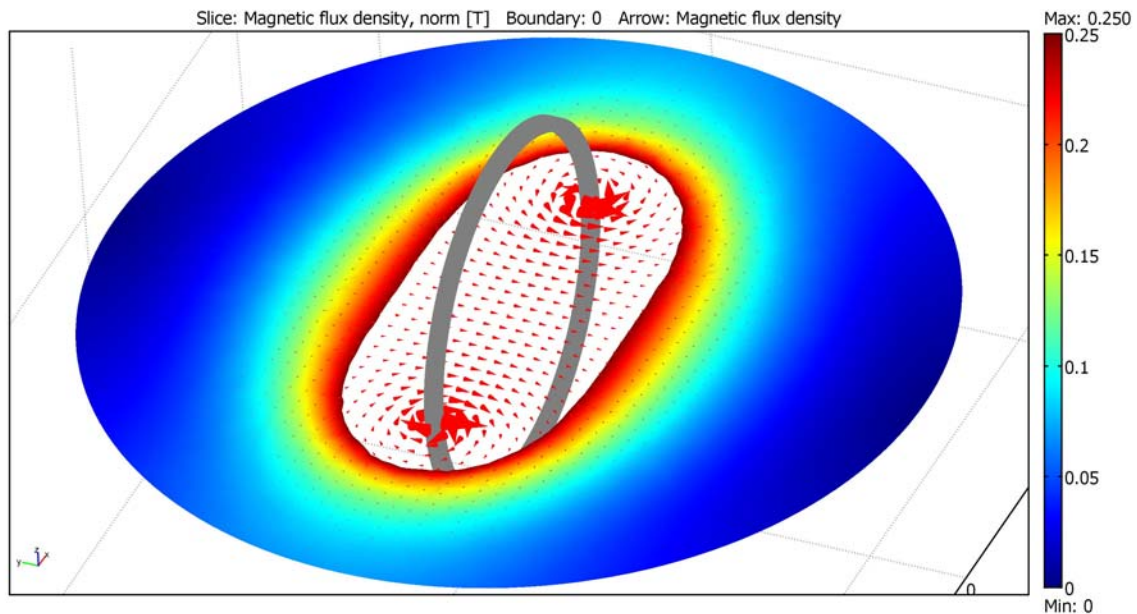


Figure 8. Typical model output

For the electromagnet, coil dimensions and the peak current were known and could be input into COMSOL. In addition to the initial conditions, grid discretisation is another parameter that needed to be selected. Several options are available for grid sizing and these were explored to determine an appropriate value. It was found that an 'extra fine' mesh size provided adequate results without impacting on run time or hardware limitations. Table 4 shows how field calculations at two arbitrary locations (0,0,0) and (0,0,100) in model Type A, for an 82 kA current, varied with grid size and the consequent run time. A finer mesh setting was available, however, this was found to be beyond the capabilities of our hardware. Table 5 shows that the magnetic field predicted by COMSOL was a good approximation to the analytical solution for an 'extra fine' mesh size when using Eq 1.

Table 4. Effect of grid size on calculated values and runtime

Mesh Size	Mesh Elements	$B_z(0,0,0)$ (T)	$B_z(0,0,10)$ (T)	Solution Time (s)
Coarse	9,870	0.66	0.34	108
Normal	20,074	0.67	0.34	146
Fine	32,089	0.67	0.34	170
Finer	84,759	0.68	0.35	235
Extra Fine	352,742	0.77	0.40	1067
Analytical	N/A	0.78	0.40	N/A

An idealised type A coil was modelled as shown in Figure 9. For this case the modelling domain extended to ~600 mm to be able to provide calculated values for comparison. Figure 9 shows the magnetic field strength along a slice in the XZ plane. The colours represent the total

magnetic field strength up to 0.1 T, with the scale shown in the colour bar. At the region around the centre of the coil, the field strength exceeds 0.1 T, displaying this region as white. The size and orientation of the arrows represent the field strength and direction at that point respectively.

As the physical coil is not well represented by an ideal coil, the sensitivity of the solution to a number of coil setup parameters was explored. Parameters used to adjust the calculated field were coil out of plane rotation and coil misalignment. Only small variations were investigated: angular misalignment of 5° for type A, 5° and 10° for type B, and a lateral misalignment of 10 mm for type B coil only.

Table 5 lists the range of solutions (minimum to maximum) found from the parameter sensitivity study and compares these values with measured data for Type A and B coils at several distinct points. For the type A coil the points were (100,0,-680), (0,100,-680), (-100,0,-680), (0,-100,-680), and (0,0,-260), and (0,0,0) – *front face of coil* and for the type B coil the points were (100,0,-510), (0,100,-510), (-100,0,-510), (0,-100,-510), (0,0,-75), (0,0,155), and (0,0,-155) – *later two being top and bottom edge of coil pair*.

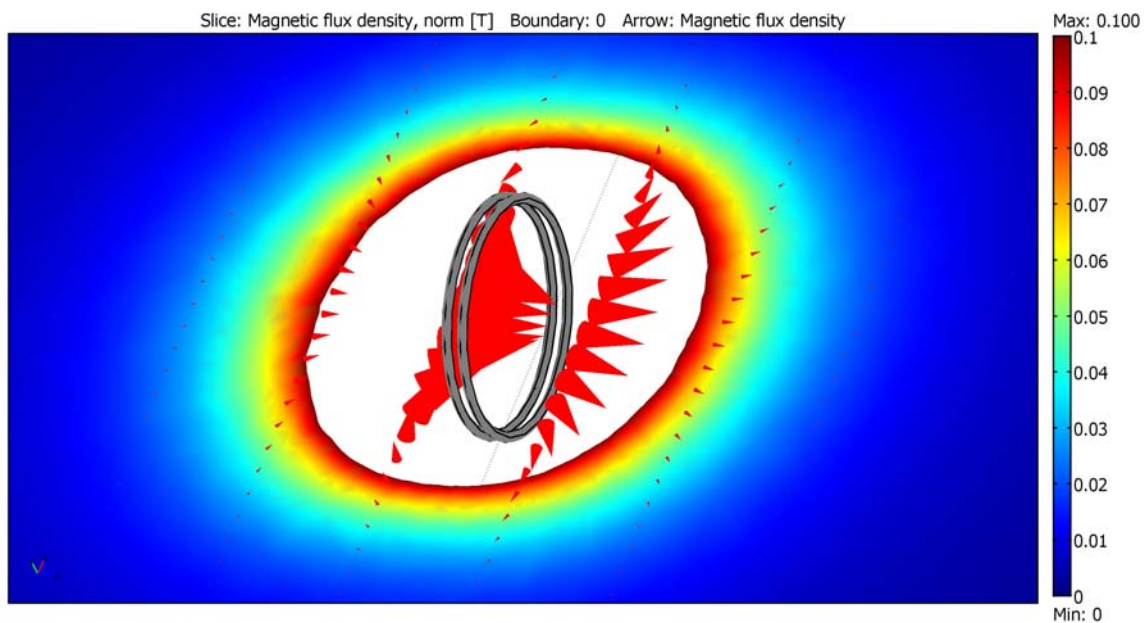


Figure 9. Example of a coil model for COMSOL

Table 5 Comparison of COMSOL and experimental data for type A and B coils. Footnotes are the same as for Table 3.

Coil	x (mm)	y (mm)	z (mm)	Current (kA)	B _{total} min (mT)	B _{total} max (mT)	Measurement (mT)
A	100	0	-680	81	4.3	4.4	9.4
A	0	100	-680	86.5	4.6	4.7	10.1
A	-100	0	-680	81	4.3	4.4	11.2
A	0	-100	-680	83	4.4	4.5	10.8
A	0	0	0	93	831	851	1020 ¹
A	0	0	-260	93	67	74	94 ¹
B	100	0	-510	99.3	6.7	7.3	8.8
B	0	100	-510	97	7.6	7.9	10.4
B	-100	0	-510	99.3	7.3	7.6	11.2
B	0	-100	-510	96.7	7.6	7.8	11.1
B	0	0	0	95	268	280	298 ²
B	0	0	-75	95	220	227	307 ³
B	0	155	0	95	623	674	697 ²
B	0	-155	0	95	622	681	667 ²

The predictive model developed to explore the spatial and temporal structure of the field due to an electromagnet was used to determine the theoretical capability of our PPS. To assist in this the unclamped time varying current from an LRC circuit (L is the inductance, R is the resistance, and C is the capacitance) as given by Eq 2, where V_0 is the charge voltage, ω is the angular frequency (a function of L , R , and C), and t is the time was used.

$$i(t) = \frac{V_0}{\omega L} e^{-\frac{Rt}{2L}} \sin(\omega t) \quad (2)$$

And where the peak current, i_p

$$i_p = \frac{V_0}{\omega L} e^{-\frac{R\pi}{4\omega L}} \quad (3)$$

The clamping diode employed in the PPS actually changes those functions by limiting the reverse current as shown in Figure 6, and in so doing also reduces the theoretical peak current. Our observations indicate that the reduction can be as much as 30%.

Conservative circuit parameters for our PPS were: $V_0 = 10$ kV, $L = 6.5$ μ H, $R = 6.5$ m Ω , and $C = 3000$ μ F for both coils which means a conservative peak current of ~ 135 kA. Eq 1 was used to determine that ~ 130 kA is required to achieve a ~ 1 T field at 50 mm from the centre of a type A coil. Using Eq 2 the duration over which this current is satisfied turns out to be ~ 78 μ s. Modifying Eq 1 to account for the coil pair in the type B coil it was determined that only ~ 0.39 T (coil centre to centre distance is ~ 367 mm) was possible at the centre of the coils for

the maximum conservative current of 135 kA. Figure 10 plots the growth of the field as a function of time for the two coil types (at the two defined locations). Figure 13 shows the spatial field distribution in the YZ plane through the centre of the type A and B coils at 220 μs (the estimated time of peak current).

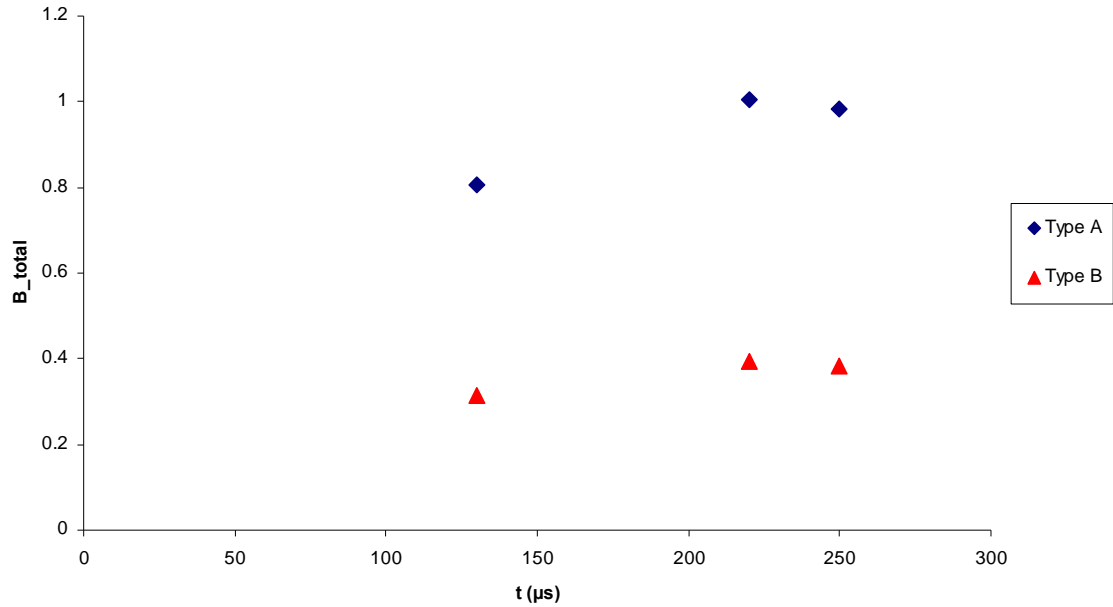


Figure 10. Predicted field growth and decay as a function of time for $V_0=10$ kV, $L=6.5$ μH , $R=6.5$ $\text{m}\Omega$, and $C=3000$ μF for (0,0,-20) and (0,0,0) for type A and B coils respectively

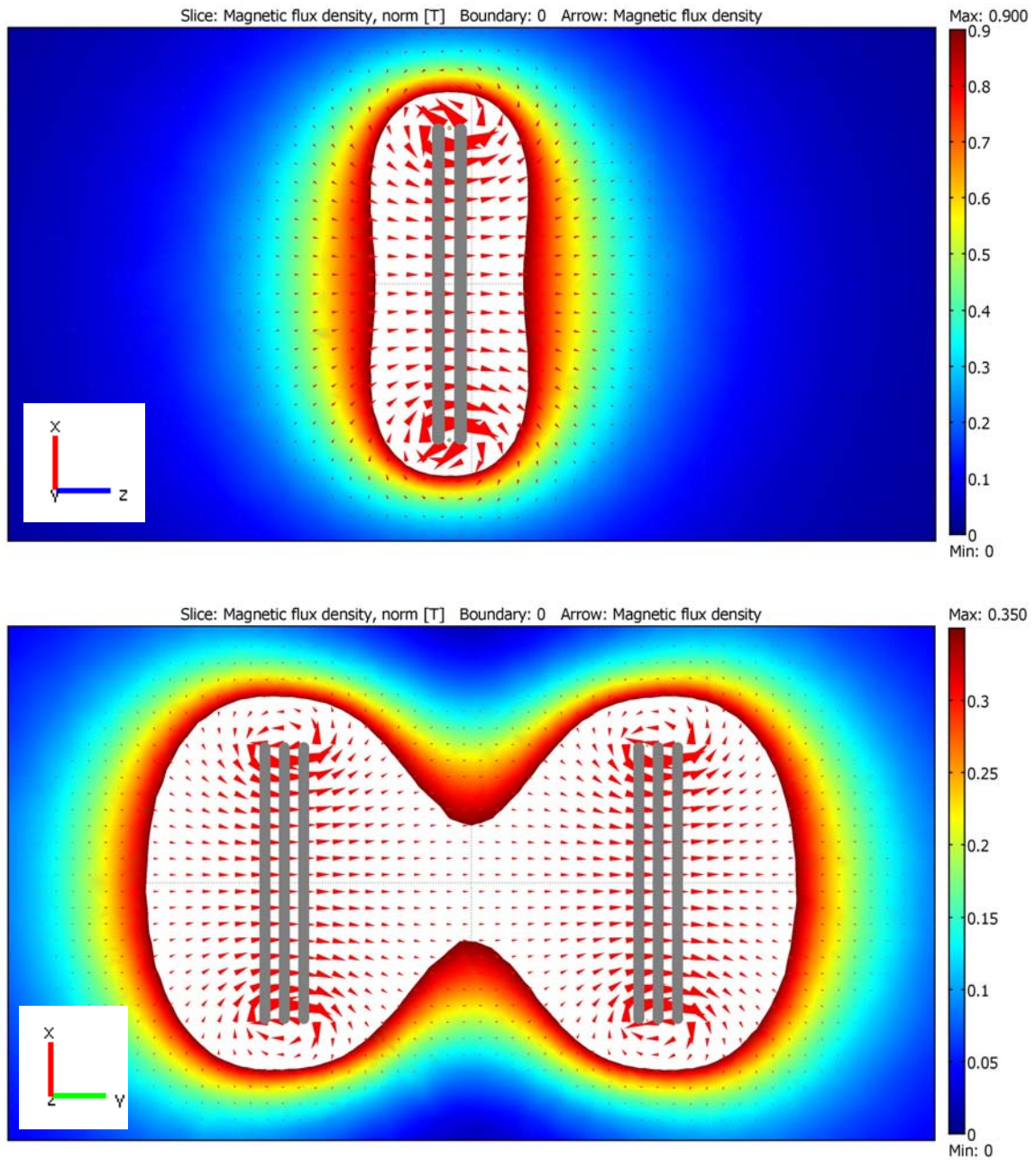


Figure 11 spatial field distribution in the YZ plane through the centre of the type A and B coils at $220 \mu\text{s}$. Note that the field strength colour bar is set to a maximum of 0.9 T for the type A coil and 0.35T for the type B coil.

4. Discussion

The field measured around the disc magnet shows some surprising features. There appears to be an anomaly between (0,0,0) and (20,0,0) and there are polarity changes at the longer ranges – refer Table 2a. Reasons for the asymmetrical behaviour and polarity changes may relate to sensor placement error, sensor accuracy, and inherent asymmetry in the magnet construction. A 3-axis probe would have been more useful and may have reduced the measurement location errors. This field cannot be easily accommodated in our modelling, however, Figure 7 does show good agreement can be achieved with our simple approach over a small region. In addition, the methodology developed to collect the data and build a model proved to be a useful starting point for the more complicated problem associated with the electromagnet.

The electromagnets were difficult to build uniformly. For example a symmetric coil is difficult to wind with these thick cables moving out of the starting plane as the coil is wound. At the end of the coil there is either a cable crossover or an incomplete circle constructed and there are asymmetrical features added by the feed in connections. For two coils as per the Helmholtz-like pair, the problems are exacerbated because in addition to the above, there are the added issues of coil angular and lateral misalignment. The result is that the real coils cannot be represented as idealised coils and are not amenable to an analytical solution. It is therefore not surprising that the measured fields were not symmetric although Table 3 shows that the deviations are not great. Careful build by using solid, possibly machined helices with well defined feed in connections, can improve the symmetry to an extent, however, as these coils were intended to be used in a potentially destructive environment it was determined that a more important requirement was ease of manufacture provided the fields could be reasonably symmetric and the magnetic field strength sufficiently intense.

Concerns surrounding the symmetry of the coil were a significant reason for conducting the field measurements and subsequent modelling. Measurements would ideally be conducted using a 3 axis probe near the region of interest, however, apart from the single axis teslameter probe, this was generally not possible or practical, and so the far field measurements were used to evaluate near field symmetry as well as to support validation of the near field predictions.

Table 5 shows that the far field measurements are generally greater than the modelled values. This systematic difference could be a result of operating the sensor in a non-linear range, but moving the field source even further away was not practical. While the absolute values are not consistent, the measurements do indicate the same order of magnitude and therefore provide confidence that the source is reasonably symmetrical and that the model provides a good spatial field representation.

The off-axis near field measurement is consistent with a uniform central field for the type B coil. All near field measurements are generally higher than the modelled values. One reason for the discrepancy between model and measurement could be related to the simple model employed. Some of those limitations have already been explored in Table 5, however, another possible source of departure could be due to disregard of the field contributions from the connection cables and other nearby conductors.

Even with the given assumptions and limitations, it seems that the modelling provided a reasonable estimate of the field in the region of interest. It is also worth noting that the field is not significantly affected by the small perturbations investigated.

The measurement and modelling have confirmed that a 1 T field could be constructed near the single coil electromagnet for approximately 78 μs and have demonstrated that prediction of the spatial distribution of that field was also possible. In addition, the modelling showed that the PPS was probably at the limit for producing such intense fields, particularly for the Helmholtz like pair. With respect to field duration, it is interesting to note that the oscillating current decay due to the diode clamp, as shown in Figure 6, has the effect of slowing the field collapse, which benefits the experimental setup as the intention is to maintain a strong field for as long as possible.

The model could be improved to achieve even better matching by creating a more realistic representation of the coil set up. Indeed, the superposition principle of electromagnetic fields means that the effect of connection cables could be added to this model relatively easily. A more complete remodelling would require significant effort that could be undertaken as an extension of the current work.

Despite the shortcomings of the magnetic field characterisation, it was shown that the model provides a realistic representation suitable for the task at hand and could be used to predict the field at any location within the domain of interest.

5. Conclusion

A methodology to evaluate the spatial and temporal magnetic field distribution around two different field sources has been developed and assessed. The approach has been found to provide a reasonable characterisation of the field that was useful for the requirements of the task. Various improvements to the model could be implemented, however, these would require significantly more effort to achieve. Any endeavour to improve future modelling would require an associated undertaking focused on achieving more accurate field measurements.

6. Acknowledgements

An experiment such as this requires several support staff. The authors wish to thank Mike Wood for use of the PPS. Funding from ONR contract N00014-09-C-0032 is acknowledged.

7. References

1. J. Waschl, F. J. Melia, and E. Todd. Magnetic Field Interaction with Detonation Products. DSTO-RR-0354. April 2010.
2. <http://www.kjmagnetics.com/>
3. <http://www.magneticosciences.com/>
4. Design of a Pulsed-Power System. M. Wood and J. Waschl. DSTO-CR-2011-0095. April 2011.
5. http://www.gmw.com/magnetic_sensors/sentron/csa/MFS3A.html
6. COMSOL Multiphysics. Version 3.5a. AC/DC Module

Appendix A: COMSOL input file for all models

Magnetic Field of Helmholtz Coil – page 97 , AC/DC Module Model Library, COMSOL version 3.3, August 2006.

The tutorial can also be accessed within COMSOL by selecting

Model Library -> AC/DC Module -> Electrical Components -> Helmholtz coil

The Magnetic Field of a Helmholtz Coil model was used as a starting point for the construction of all models. Aside from geometric parameters, the model was setup as in the tutorial, with all coils being modelled in the x-y plane, apart from the single disc magnet which was modelled in the x-z plane. Geometric parameters were altered to match the configuration as accurately as possible .

The models where the coils were rotated by either 5° or 10° required the current density vector J listed on page 102 to be modified. The vector J was multiplied by the three dimensional rotation matrix to find the new current density vector.

Rotation matrix R, for an angle of rotation of α radians clockwise about the y-axis.

R =

$\cos \alpha$	0	$-\sin \alpha$
0	1	0
$\sin \alpha$	0	$\cos \alpha$

The rotation matrix was applied to the current density vector to give the rotated current density vector.

$$J_{\text{rotated}} = \left[\frac{-J_0 * y * \cos \alpha}{\sqrt{x^2 + y^2}}, \frac{J_0 * x}{\sqrt{x^2 + y^2}}, \frac{J_0 * y * \sin \alpha}{\sqrt{x^2 + y^2}} \right]$$

The rotated current density was then applied to the coil that was geometrically rotated about the y-axis.

For the Helmholtz model, the coordinate system in COMSOL that the coil was modelled in was different to the actual coordinate system defined for the coil in Figure 5. To convert between the coordinate systems the following table was used

Coordinate System	COMSOL
Bx	Bx
By	Bz
Bz	-By

To create the misalignment model one of the two coils in the type B model was translated by 10 mm in the negative x-direction. The current density vector needed to be adjusted for this translation by replacing the 'x' coordinate with 'x+0.01'. The current density vector used for the misaligned coil was $J_{\text{misaligned}}$

$$J_{\text{misaligned}} = \left[\frac{-J_0 * y}{\sqrt{(x + 0.01)^2 + y^2}}, \frac{J_0 * (x + 0.01)}{\sqrt{(x + 0.01)^2 + y^2}}, 0 \right]$$

The current density vector in the other of the two coils was defined as:

$$\left[\frac{-J_0 * y}{\sqrt{x^2 + y^2}}, \frac{J_0 * x}{\sqrt{x^2 + y^2}}, 0 \right]$$

